PL-TR-92-2022

APPLICATION OF IRIS/IDA STATIONS IN THE USSR TO SEISMIC MONITORING RESEARCH:

The Use of Velocity Spectrum in the Stacking of Receiver Functions with Application to IRIS Station at Obninsk, USSR

H. Gurrola
J.B. Minster
T. Owens
H.K. Given

University of California San Diego
Institute of Geophysics and
Planetary Physics
Scripps Institution of Oceanography
La Jolla, CA 92093-0225

15 January 1992

Scientific Report No. 1

PHILLIPS LABORATORY
AIR FORCE SYSTEMS COMMAND
HANSCOM AIR FORCE BASE, MASSACHUSETTS 01731-5000

The views and conclusions contained in this document are those of the authors and should not be interpreted as representing the official policies, either expressed or implied, of the Air Force or the U.S. Government.

This technical report has been reviewed and is approved for publication.

JAMES F. LEWKOWICZ
Contract Manager
Solid Earth Geophysics Branch
Earth Sciences Division

JAMES F. LEWKOWICZ
Branch Chief
Solid Earth Geophysics Branch
Earth Sciencs Division

DONALD H. ECKHARDT, Director
Earth Sciences Division

This document has been reviewed by the ESD Public Affairs Office (PA) and is releasable to the National Technical Information Service (NTIS).

Qualified requestors may obtain additional copies from the Defense Technical Information Center. All others should apply to the National Technical Information Service.

If your address has changed, or if you wish to be removed from the mailing list, or if the addressee is no longer employed by your organization, please notify PL/IMA, Hanscom AFB MA 01731-5000. This will assist us in maintaining a current mailing list.

Do not return copies of this report unless contractual obligations or notices on a specific document requires that it be returned.

REPORT DOCUMENTATION PAGE

Form Approved
OMB No. 0704-0188

1. AGENCY USE ONLY (Leave blank)	2. REPORT DATE	3. REPORT TYPE AND DATES COVERED
	15 January 1992	Scientific Report No. 1

4. TITLE AND SUBTITLE
Application of IRIS/IDA Stations in the USSR to Seismic Monitoring Research: The Use of Velocity Spectrum in the Stacking of Receiver Functions With Application to IRIS Station at Obninsk, USSR

5. FUNDING NUMBERS
PE 62101F
PR 7600 TA 09 WU BD
Contract F19628-90-K-0045

6. AUTHOR(S)
H. Gurrola T. Owens
J.B. Minster H.K. Given

7. PERFORMING ORGANIZATION NAME(S) AND ADDRESS(ES)
University of California, San Diego
Institute of Geophysics & Planetary Physics
La Jolla, CA 92093-0225

8. PERFORMING ORGANIZATION REPORT NUMBER

9. SPONSORING/MONITORING AGENCY NAME(S) AND ADDRESS(ES)
Phillips Laboratory
Hanscom AFB, MA 01731-5000

Contract Manager: James Lewkowicz/GPEH

10. SPONSORING/MONITORING AGENCY REPORT NUMBER
PL-TR-92-2022

11. SUPPLEMENTARY NOTES

12a. DISTRIBUTION/AVAILABILITY STATEMENT
Approved for public release;
Distribution unlimited

12b. DISTRIBUTION CODE

13. ABSTRACT *(Maximum 200 words)*
In order to improve the signal-to-noise ratio of receiver function data, it is typical to stack receiver functions calculated from events at similar distances and back azimuths. We have adapted the velocity spectrum stacking technique, used extensively in reflection seismology, to the receiver function method in order to stack data with different ray parameters, thereby improving further the signal-to-noise ratio. Perhaps more importantly, by producing the velocity spectrum stacks we take advantage of the differences in the shapes of the moveout curves of converted phases and reverberations to identify and separate the various phases and to infer velocity structure. Through conventional receiver function techniques we have modeled the crustal structure beneath the IRIS/IDA seismographic station at Obninsk, Russia. This model includes a low-velocity, 2 km thick surface layer, and a 47 km depth to Moho with relatively uncomplicated crustal structure. By comparison of the velocity spectrum stacks produced from the observed data at Obninsk with those produced from PREM synthetics we have identified Ps phases from the 410 and 670 km discontinuities. We find no evidence of a 210 km discontinuity beneath Obninsk in the receiver function data.

14. SUBJECT TERMS		15. NUMBER OF PAGES
Seismology	Magnitude	30
USSR	Crustal structure	16. PRICE CODE
Regional phases	Mantel structure	

17. SECURITY CLASSIFICATION OF REPORT	18. SECURITY CLASSIFICATION OF THIS PAGE	19. SECURITY CLASSIFICATION OF ABSTRACT	20. LIMITATION OF ABSTRACT
Unclassified	Unclassified	Unclassified	SAR

The Use of Velocity Spectrum in the Stacking of Receiver Functions with Application to IRIS Station at Obninsk, USSR

H. Gurrola,[1] J. B. Minster,[1] and T. Owens[2]

[1] *Institute of Geophysics and Planetary Physics, University of California at San Diego, La Jolla, CA, 92093*

[2] *Department of Geological Science, University of South Carolina, Columbia, SC, 29208*

SUMMARY

In order to improve the signal to noise ratio of receiver function data, it is typical to stack receiver functions calculated from events at similar distances and back azimuths. We have adapted the velocity spectrum stacking technique, used extensively in reflection seismology, to the receiver function method in order to stack data with different ray parameters, thereby improving further the signal to noise ratio. Perhaps more importantly, by producing the velocity spectrum stacks we take advantage of the differences in the shapes of the moveout curves of converted phases and reverberations to identify and separate the various phases and to infer velocity structure. Through conventional receiver function techniques we have modeled the crustal structure beneath the Soviet IRIS seismographic station at Obninsk. This model includes a low velocity 2 km thick surface layer and 47 km depth to Moho with relatively uncomplicated crustal structure. By comparison of velocity spectrum stacks produced from the observed data at Obninsk with those produced from PREM synthetics we have identified Ps phases from the 410 and 670 km discontinuities. We find no evidence of a 210 km discontinuity beneath Obninsk in the receiver function data.

Key words: receiver function, Obninsk, velocity spectrum stack, normal moveout, upper mantle discontinuity.

INTRODUCTION

A commonly used technique to estimate crust and upper mantle structure from a single three-component seismographic station is to compute and interpret "receiver functions" (e.g., Langston 1989, 1981, 1979, 1977; Owens, Crosson and Hendrickson 1988; Owens and Crosson 1988; Owens, Taylor and Zandt 1987; Owens, Zandt and Taylor 1984), wherein the horizontal components are deconvolved by the vertical component to produce a trace consisting primarily of

Ps conversions and converted S-wave reverberations. The technique has been successfully extended to arrays of broadband portable stations by Owens et al. (1988a,b). To improve the signal to noise ratio, receiver functions can be binned by ray parameter and back azimuth and stacked (Owens, Taylor and Zandt 1983; Owens 1984). In areas with flat geological structure the receiver functions show little or no azimuthal dependence and can be stacked at common ray parameter for all azimuths. However, if we wish to stack traces with different ray parameters, we must first correct for the differences in relative arrival times.

The "velocity spectrum stack" (VSS) is a useful tool for stacking reflection data within a range of ray parameters in multichannel studies (e.g. Yilmaz 1987). The functional dependence of arrival times on ray parameter p, relative to a reference phase with ray parameter p_0 is called the "moveout". The "normal moveout correction" (NMO) then refers to the time adjustment necessary to correct the arrival time to what would have been observed from a vertically incident ray, irrespective of amplitude, assuming a given velocity structure. The "velocity spectrum stack" is a contour map of amplitudes across constant velocity stacks (produced by stacking the observed records after NMO assuming a uniform velocity) in the velocity-time plane (e.g. Sheriff 1982). A phase present in the receiver functions is thus enhanced if the appropriate NMO correction is made. The enhancement will be most effective for a value of velocity matching the "true" mean velocity sampled by the phase. It is most appropriate at this point to think of the velocity structure as a function of time since arrival time is observed whereas depth will be computed after the velocity structure is determined (Yilmaz 1987). Because of differences in the shapes of their moveout curves, separate stacks must be produced for each of the prominent phases present in the receiver functions. Therefore, the velocity spectrum stacks can be used to distinguish between phases as well as to infer velocity structure.

The examples in the following sections, describing the production of VSS, use radial components of the receiver functions. Since the production of the VSS depends only on travel time, the tangential component VSS can be produced using the same procedure, however for 1-dimensional structure there will be no energy on the tangential components.

METHOD

Figure 1 illustrates the geometry of the most significant type of phase observed in receiver function studies - the P to S conversion (Ps) generated when the wave crosses an interface - for a layer over a half space. The time delay for the Ps arrival relative to that of the P arrival $\Delta T_{Ps}(p)$ is given by:

$$\Delta T_{Ps}(p) = T_S + T_h - T_P \quad (1)$$

$$\Delta T_{Ps}(p) = z\left(\sqrt{V_S^{-2} - p^2} - \sqrt{V_P^{-2} - p^2}\right) \quad (2)$$

In the above equations: T_S, T_h and T_P are travel times along the paths labeled in Figure 1; V_S and V_p are the average S and P velocities in the layer, respectively; p is the ray parameter; and z is the depth to the interface. In terms of the vertical travel time of Ps relative to P (ΔT_{Ps0}) through the layer and the velocity ratio $r = V_p / V_s$, we have:

$$\Delta T_{Ps}(\Delta T_{Ps0}, p, V_S, r) = \frac{r\Delta T_{Ps0}}{r - 1}\left(\sqrt{1 - p^2V_S^2} - \sqrt{r^{-2} - p^2V_S^2}\right) \quad (3)$$

Note that this equation depends only on ΔT_{Ps0}, p, V_S and an assumed value for r (which will be held constant for an entire velocity spectrum stack, e.g. $r=\sqrt{3}$ for a Poisson solid). Figure 2 depicts a set of synthetic receiver functions generated for a layer (V_P = 6.0 km/sec, V_S = 3.5 km/sec) over a half space (V_P = 8.0 km/sec, V_S = 4.6 km/sec, and z = 40 km) for a range of ray parameters. We see that the Ps phase is delayed with increasing ray parameter relative to the initial P-wave, illustrating the Ps moveout. All phases (reverberations) following Ps are advanced in arrival time relative to the P phase with increasing ray parameter. The next prominent phase after the Ps arrival is composed of the sum of all reverberations in which there are two P legs and one S leg. Figure 3 depicts the travel path of the Ppps phase in which the first two branches are P waves and the final branch is an S. For near vertical incidence the reverberations ending in an S branch will contribute much more energy to the horizontal components than those ending in a P (ie. Pspp, and Ppsp). For convenience of notation we will adopt a naming convention for the sum of these reverberations as Pnpms, in which n is the number of p legs and m is the number of s legs (if n or m is zero it is omitted). The phase described will be refered to as P2p1s. The next phase on Figure 2, P1p2s, composed of the sum of reverberations with two S legs and one P, has two contributions with final S legs (the Psps and Ppss) and a less significant Pssp contribution.

We take advantage of this difference in the shape of the moveout curve to distinguish reverberations from the Ps phase. Equation 4 gives the time delay (ΔT_{P2p1s}) for the P2p1s phase relative to the P arrival for a layer over a half space:

$$\Delta T_{PPS}(\Delta T_{PPS0}, p, V_S, r) = \frac{r\Delta T_{PPS0}}{r + 1}\left(\sqrt{1 - p^2V_S^2} + \sqrt{r^{-2} - p^2V_S^2}\right) \quad (4)$$

In like fashion, we can derive moveout equations for the P3p, P1p2s and P3s phases. However P3p and P3s have small amplitudes (even after stacking a very large number of events) so are usually of little significance in interpretations. P1p2s, on the other hand, has reversed polarity and is easily distinguishable from Ps and P2p1s, so it is sometimes a useful phase in the interpretation of receiver structure.

Constant velocity stacks are produced by averaging along the moveout curve the amplitudes of N receiver functions with various ray parameters.

$$S(\Delta T_{\Phi 0}, V_s) = \frac{1}{N} \sum_{i=1}^{N} f_i\{\Delta T_\Phi(\Delta T_{\Phi 0}, p_i, V_S, r)\} \qquad (5)$$

Where Φ is the type of phase (ie. Ps or P2p1s); $S(\Delta T_{\Phi 0}, V_s)$ is the averaged amplitude at a given zero offset time and S-wave velocity; $f_i\{\Delta T_\Phi(\Delta T_{\Phi 0}, p_i, V_s, r)\}$ is the amplitude of the i^{th} trace at the computed moveout time, $\Delta T_\Phi(\Delta T_{\Phi 0}, p_i, V_s, r)$, for a given wave type (Φ). If the moveout time falls between two samples we linearly interpolate a value for $f_i\{\Delta T_\Phi(\Delta T_{\Phi 0}, p_i, V_s, r)\}$. After producing constant velocity stacks for the range of all reasonable velocities, we contour the amplitudes in the velocity-time plane to produce the "velocity spectrum stack" (VSS). The Ps conversion or P2p1s reverberation on their respective velocity spectrum stacks will appear as positive ridges (negative for a velocity inversion) elongated parallel to the velocity axis. The velocity structure beneath a station can then be inferred by selecting the time and velocity of the highest amplitude on each ridge.

A SYNTHETIC EXAMPLE

Figure 4 depicts VSS produced for the Ps and P2p1s phases for the synthetic receiver functions shown in Figure 2. Upon inspection of the Ps stack (left) we observe good time resolution for Ps near 5 seconds but poor velocity resolution. This phase also appears on the P2p1s stack (right), but the peak is not as sharp and does not have as large an amplitude as on the Ps stack. P2p1s (at 18 sec) is only observed on the P2p1s stack and has much better velocity resolution than Ps. It is not surprising that we are able to pick V_S=3.5 km/sec (the velocity used to compute the synthetics in Figure 2) more accurately from P2p1s stack, since Figure 2 shows twice as much moveout for P2p1s than for Ps. We can use this velocity together with the approximate 4.8 sec arrival time on the Ps stack to compute the thickness of the layer. The arrival times on the VSS are zero offset arrival times, so equation (2) becomes:

$$T_{Ps}=z\{1/V_S - 1/V_P\} \qquad (6)$$

Solving for z we find a 40 km depth to Moho.

Figure 5 depicts single stacks of the receiver functions shown in Figure 2. The top stack has no moveout applied - the next three are stacked using the respective Ps, P2p1s, and P1p2s moveout curves (from top to bottom). In each case the respective velocity depth (time) function was picked by observation of the stacking amplitudes on the corresponding VSS (Figure 4). The P, Ps, P2p1s, and P1p2s arrivals are at 5, 10, 23 and 28 seconds respectively. Figure 5 clearly illustrates the fact that the various arrivals are substantially enhanced when stacked under the appropriate moveout curve. An added bonus is the annihilation of the reverberations (P2p1s and P1p2s) on the Ps stack and conversely the Ps phase is greatly diminished on the two reverberation stacks. We conclude that by producing the stacks with normal moveout we may observe arrivals that would otherwise be below noise levels and avoid mislabeling other phases.

Figures 6 and 7 depict the shape of the Ps and P2p1s moveout curves computed for various depths using the PREM velocity model (Dziewonski and Anderson, 1981) over the range of ray parameters typical of P-arrivals used in receiver function studies (0.04 to 0.08 sec/km or an arc distance of 30° to 90°). For an interface depth of 50 km, there is 0.75 sec. of moveout over this range of ray parameters. There is about 2.5 sec. of moveout calculated over the same range of ray parameter for the P2p1s phase at the 50 km depth. We observed in Figure 4 that for an even shallower depth (40 km.), with less moveout, reasonable signals appeared on the VSS for both phases. For the Ps phase, there are 1.8 sec. of moveout at 100 km and at 600 km there are 16.1 sec. of moveout over the range of ray parameters. It is clear that with a finite number of traces to stack VSS produced for the Ps phase will be much more useful in the interpretation of upper mantle structure than for crustal structure.

On the other hand, about 1.25 seconds of moveout is expected for the P2p1s over the given range of ray parameter at the 25 km depth. Because of the greater amount of moveout observed for this phase their VSS may prove to be more valuable in the interpretation of shallow structure. The longer ray path of the reverberations (as opposed to the direct Ps) make this phase more sensitive to heterogeneities in the near surface structure. As a result interpretation of these phases may be more difficult (Owens et al. 1984).

It is clear from Figure 6 that to produce reliable VSS for shallow layers (100 km or less), data from the full range of ray parameters are necessary. For the Ps phases from deeper interfaces and

the P2p1s phase at all depths, it appears that there is sufficient moveout along the curves to produce VSS from data with sparser distribution data than for the shallower layers. In cases where there is not enough distribution to use VSS to make a preliminary estimate of Vs, it may be desirable to restack the data after making a moveout correction (not necessarily normal moveout) using a regional velocity model in order to stack the data more coherently.

CRUSTAL STRUCTURE AT OBN

We calculated Velocity Spectrum Stacks for data recorded at the Soviet station at Obninsk (OBN). We use conventional receiver response interpretation to determine crustal structure and use the VSS method in the following section to look at upper mantle discontinuities.

We have computed receiver functions for the IRIS/IDA station at OBN using data collected in 1989-90 (Gurrola, Minster and Owens 1990a,b). The station is equipped with a broadband three-component system with response nominally flat with respect to velocity from approximately 3 mHz to 5 Hz. We used teleseismic P and PP phases which, due to the uneven distribution of source regions during the one year period covered by the data, primarily sample the northeast and southeast quadrants at all sites. It was necessary to high-pass filter most of these data in order to counter the effects of occasional nonlinear noise problems at frequencies lower than 20 mHz.

The broad band OBN receiver functions are dominated by reverberations in a shallow surface layer. In order to identify phases from deeper layers, we have reduced the contribution of the near surface layer by low-pass filtering these data with a phaseless Gaussian filter (centered at 0 Hz with a half power width of 0.6 Hz, Figure 8). The velocity structure was determined using the smooth inversion of Ammon (personal comm., 1990), which employs the reflection matrix method (Kennett, 1983, and Randall, 1989). The simplest model that we could construct which satisfies both the broad band and the high frequency data includes a low velocity surface layer of no more than 2.5 km thickness and a rather smoothly increasing velocity gradient to the 47 km deep Moho (Gurrola et al. 1990a, Figure 9).

UPPER MANTLE DISCONTINUITIES AT THE OBN IRIS/IDA STATION

VSS produced from OBN receiver functions exhibit clear arrivals from the upper mantle discontinuities. The top row of Figure 10 depicts the Ps VSS computed from synthetics produced for the PREM velocity structure modified to include the OBN crustal structure (left) and the Ps stacks computed from the observed data at OBN (right). The PREM model used to compute these synthetics was modified to include the OBN velocity structure described above. The bottom row depicts the corresponding P2p1s stacks. We observe Ps and P2p1s phases from the Moho at about 5 and 20 seconds respectively. The contour interval was chosen to illustrate best the upper mantle arrivals not observable on the individual receiver functions. As a result, the Moho arrivals are not very sharp in these plots. We chose to use a uniform Poisson ratio in computing the VSS. Had we allowed the V_P-to-V_S ratio vary with depth as given in the PREM model, all arrivals would appear slightly sooner in time and lower in velocity. The effect of this approximation will be the same on VSS computed for synthetics as for those computed for observed data and varying this ratio with depth would add another free parameter and unnecessarily complicate the interpretation.

The observed Ps phase from the 410 km discontinuity (at 42 seconds on the velocity spectrum stacks of Figure 10) exhibits much higher amplitude than the PREM synthetics. This is consistent with the larger velocity contrast for the 410 km discontinuity suggested by the K8 model of Given and Helmberger (1980). The Ps arrival from the 670 km discontinuity is similar in amplitude on both the observed stacks and the PREM synthetics, which implies a similar velocity contrast, although this arrival appears slightly earlier and at a higher velocity in the observations. The time delay between the 410 and 670 km discontinuities is smaller than observed in PREM, which is consistent with independent observations at OBN by Vinnik (personal comm., 1990).

We do not observe a 210 km discontinuity beneath OBN. The Ps phase from the 210 km discontinuity arrives just after the P2p1s from the Moho for the PREM model making the peak at 20 seconds on the synthetic velocity spectrum stacks broader than observed. The strong P2p1s arrival from the 210 km discontinuity observed at 75 seconds on the PREM VSS is not apparent in observed VSS (Figure 10). These observations lead us to conclude that there is no 210 km discontinuity beneath OBN, or at least that it is not as pronounced as in PREM.

CONCLUSIONS

Through the use of velocity spectrum stacks we can to stack data from different ray parameters, and by doing so infer velocity structure beneath the seismographic station. Velocity spectrum stacks analysis can be used to distinguish between a Ps phase and a P2p1s reverberation based on the difference in the shape of their respective moveout curves. The method looks most promising for the interpretation of upper mantle structure, however when the full range of ray parameter are available crustal phases may also be imaged with VSS.

Through the analysis of velocity spectrum stacks produced for data from OBN, we have been able to identify upper mantle Ps conversions associated with the 410 and 670 km discontinuities that were not observable in the individual receiver functions. We have also given evidence that the 210 km discontinuity is not present beneath OBN.

REFERENCES

Dziewonski, A.M. and D.L. Anderson 1981, Preliminary reference Earth model, *Phys. Earth Plan. Int.*, **25**, 297-356.

Given, J.W. and D.V. Helmberger, 1980, Upper Mantle structure of northwestern Eurasia, *Jour. of Geophy. Res.*, **85**, 7183-7194.

Gurrola, H, J.B. Minster, and T. Owens, 1990a, Receiver Responses at IRIS/IDA Stations in the USSR, 12th annual Darpa/GL Seismic Research Symposium, Geophysics Laboratory Hanscom AFB, Mass., G-L-TR-90-0212,ADA226635.

Gurrola, H, J.B. Minster, and T. Owens, 1990b, Receiver Responses at IRIS/IDA Stations in the USSR, *EOS*, 71, 1450 (abstract, S21C-12).

Langston, C.A., 1989, Scattering of teleseismic body waves under Pasadena, California, *J. Geophys. Res.*, 94, 1935-1951.

Langston, C. A., 1981, Evidence for the subducting lithosphere under southern Vancouver Island and western Oregon from teleseismic P wave conversions, *J. Geophys. Res.*, **86**, 3857-3866.

Langston, C. A., 1979, Structure under Mount Rainier, Washington, inferred from teleseismic body waves, *J. Geophys. Res.*, **84**, 4749-4762.

Langston, C. A., 1977, The effects of planar dipping structure on source and receiver responses for constant ray parameter, *Bull. Seis. Soc. Amer.*, **67**, 1029-1050.

Owens, T. J., R. S. Crosson, and M.A. Hendrickson, 1988a, Constraints on the subduction geometry beneath western Washington from broadband teleseismic waveform modeling, *Bull. Seismol. Soc. Amer.*, **78**, 1319-1334.

Owens, T. J., and R. S. Crosson, 1988b, Shallow Structure effects on Broadband teleseismic P waveforms, *Bull. Seismol. Soc. Amer.*, **78**, 96-108.

Owens, T. J., S. R. Taylor, and G. Zandt, 1987, Crustal structure at regional seismic test network stations determined from inversion of broadband teleseismic P waveforms, *Bull. Seismol. Soc. Amer.*, **77**, 631-662.

Owens, T.J., G. Zandt, S.R. Taylor, 1984, Seismic evidence for an ancient rift beneath the cumberland plateau, Tennessee: a detailed analysis of broadband teleseismic P waveforms, *J. Geophys. res.*, 89, 7783-7795.

Owens, T. J., 1984, Determination of crustal and upper mantle structure from analysis of broadband teleseismic P-waveforms, *Ph.D. Dissertation*, University of Utah, Salt Lake City, Utah, 146 pp.

Owens, T. J., S. R. Taylor, and G. Zandt, 1983, Isolation and Enhancement of the Response of Local Seismic Structure from Teleseismic Structure from Teleseismic P-waveforms, *internal report*, Lawrence Livermore Laboratory.

Randall, G. E., 1989, Efficient calculation of differential seismograms for lithospheric receiver functions, *Geophys. J. Royal Astron. Soc.*, **99**, 469-481.

Sheriff, R.E., 1982, Encyclopedic Dictionary of Exploration Geophysics, *Society of Exploration Geophysicist*, Tulsa, Ok.

Vinnik, L.P , 1977, Detection of waves converted from P to SV in the mantle, *Physics of the Earth and Planetary Interiors*, **15**, 39-45.

Yilmaz, O., 1987, Seismic data processing. *Society of Exploration Geophysicists, investigations in geophysics* volume 2.

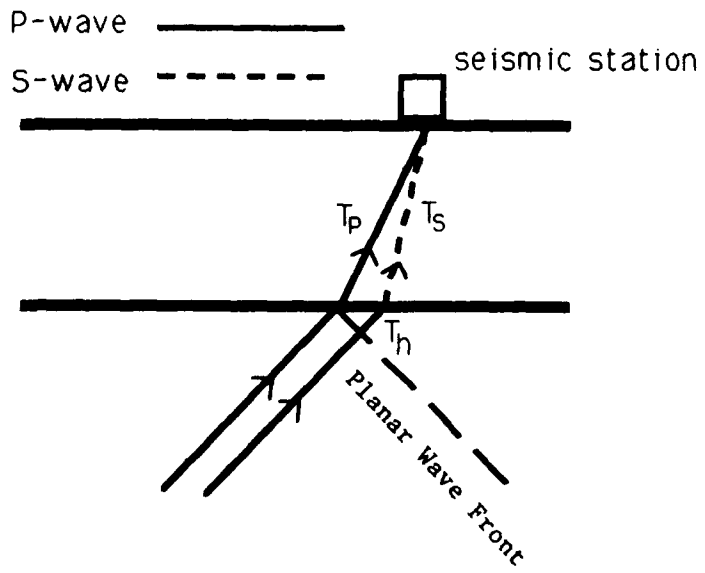

Figure 1. Ray paths for the Ps phase relative to the P phase for a layer over a half space. T_P and T_S are the travel times of the P and S phases with the same ray parameter through the layer respectively. T_h is the travel time differential in the half space for the two rays assuming a planar wave front.

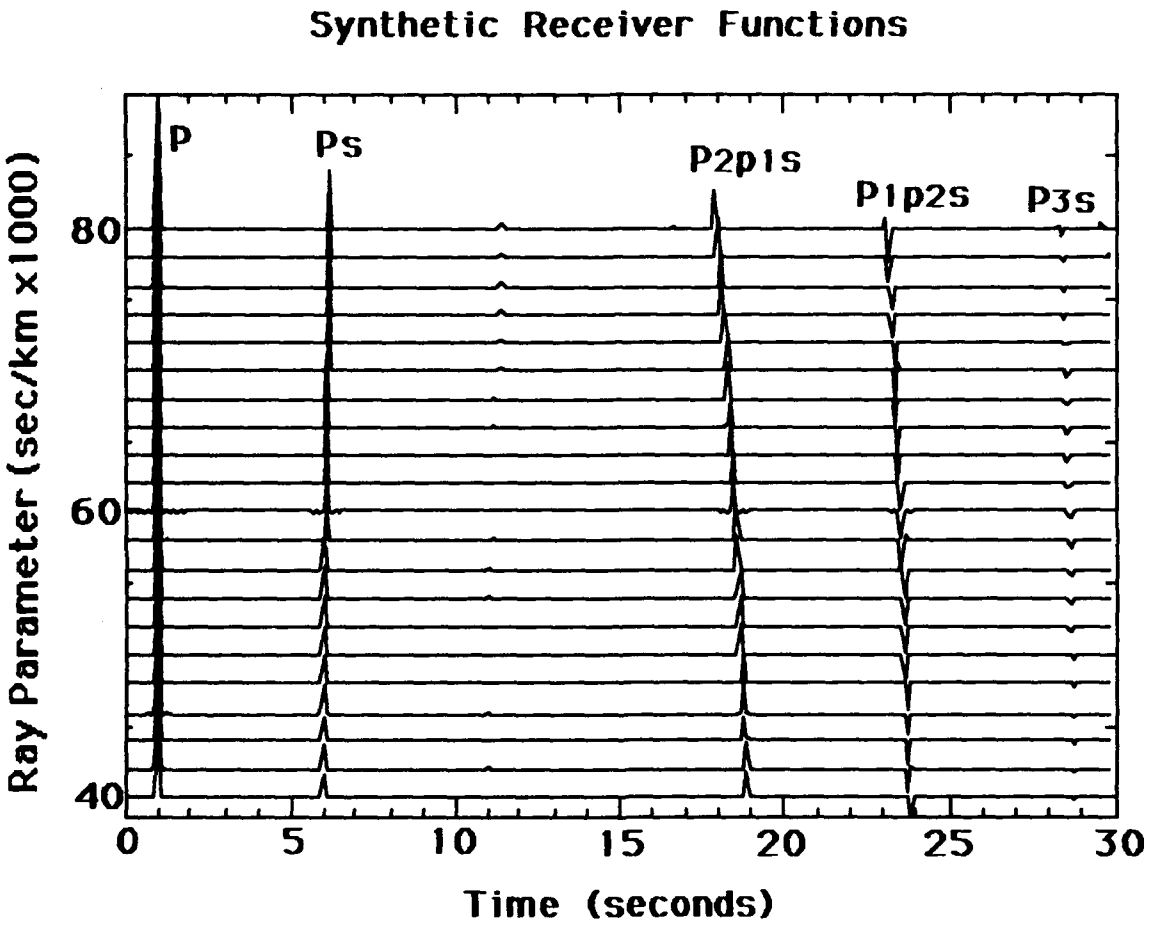

Figure 2. Seismic section of synthetic receiver functions computed for a layer (V_P=6.0 km/sec, V_S=3.5 km/sec) over a half space (V_P=8.0 km/sec, V_S=4.6 km/sec).

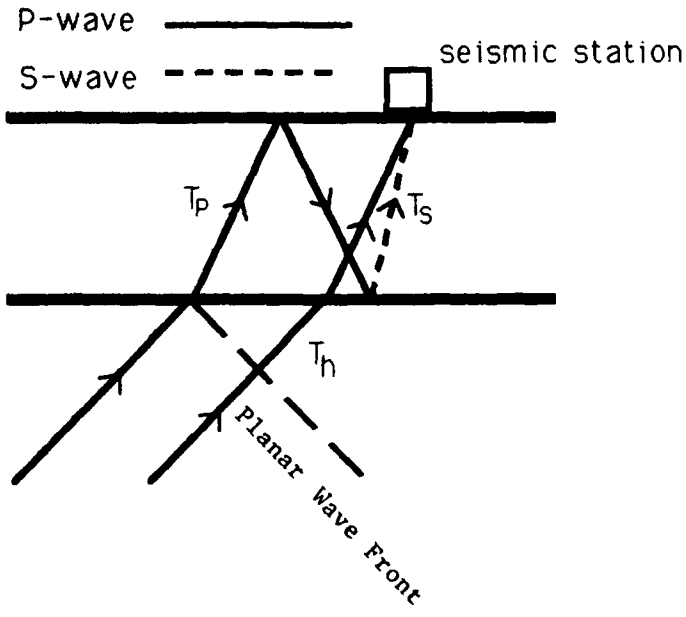

Figure 3. Ray paths for the P2p1s phase relative to the P phase for a layer over a half space. T_P and T_S are the travel times of the P and S phases with same ray parameter through the layer respectively. T_h is the travel time differential in the half space for the two rays assuming a planar wave front.

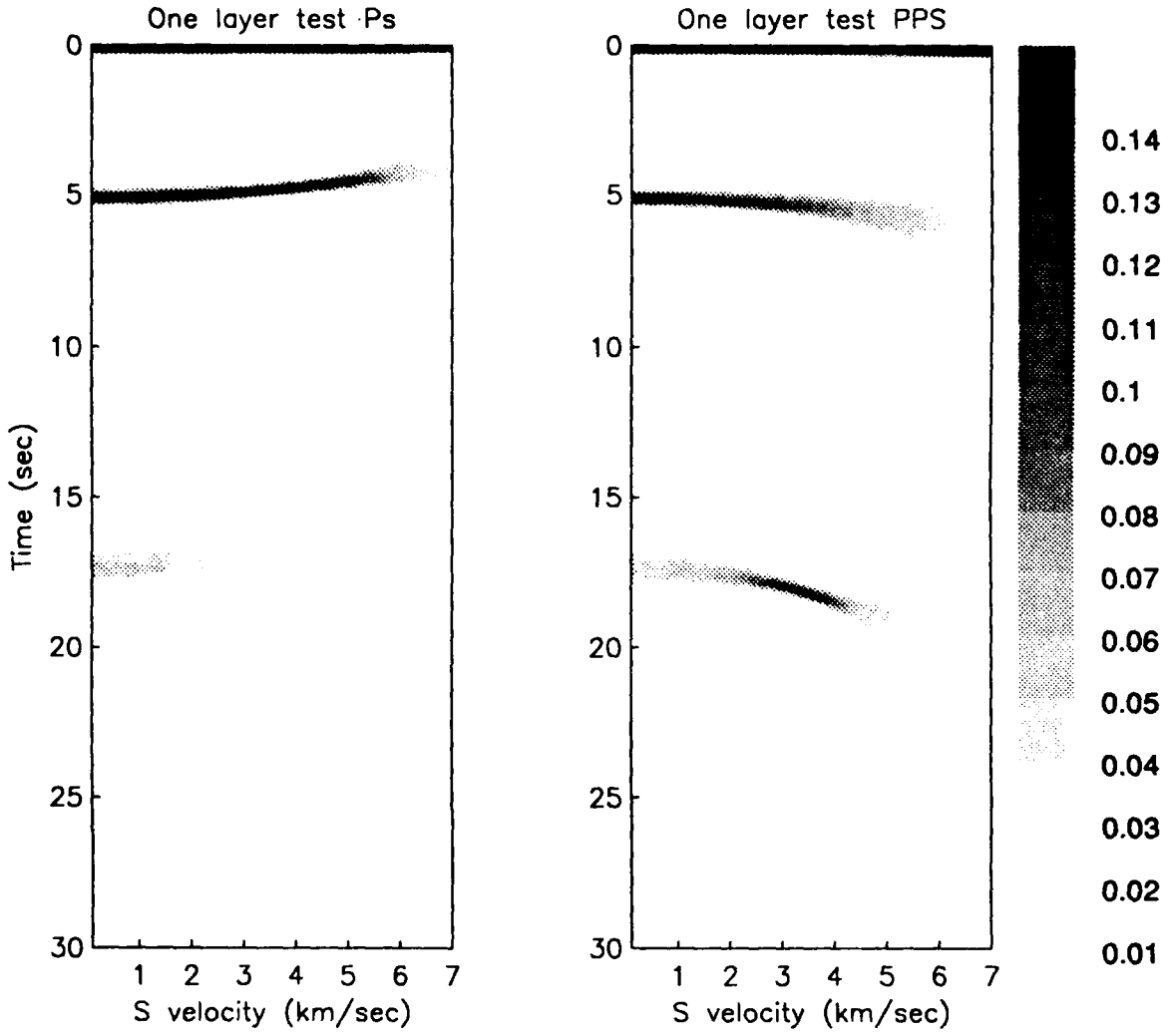

Figure 4. Velocity spectrum stacks produces from the synthetic receiver functions depicted in Figure 2. Ps stacks are shown on the left and P2p1s stacks are on the right.

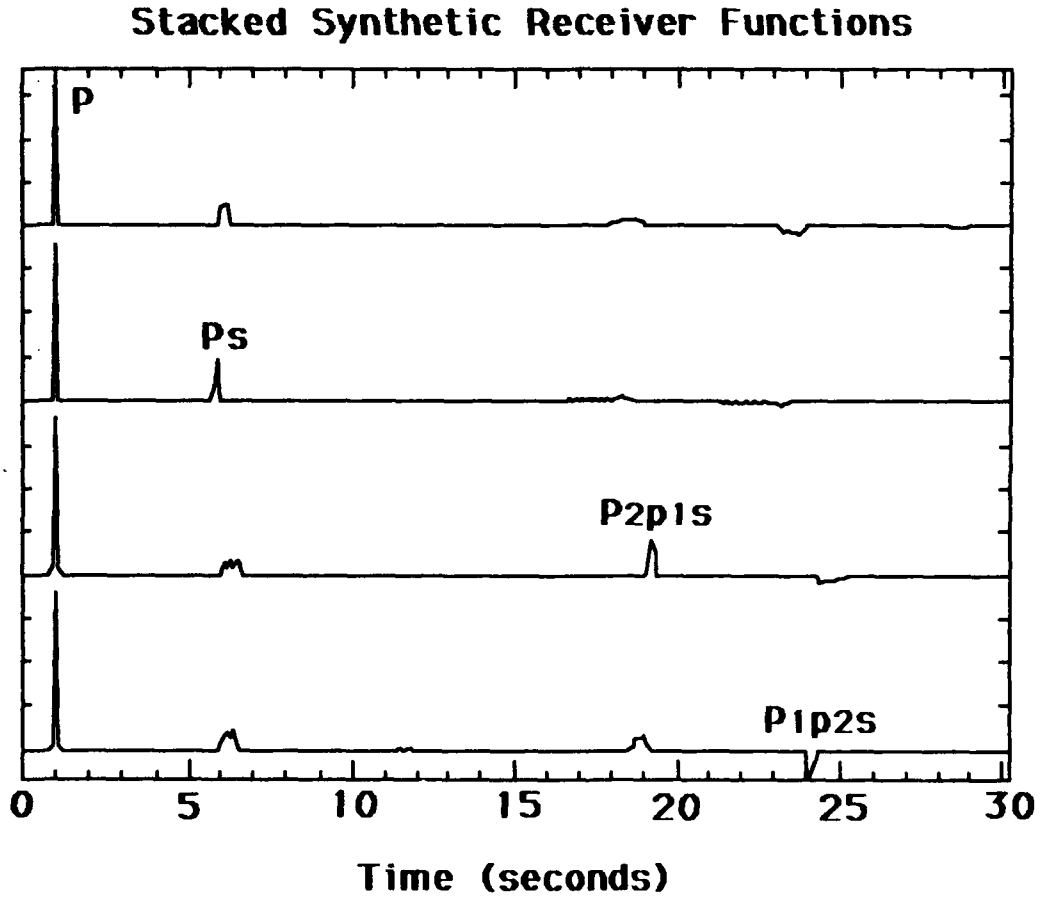

Figure 5. Stacks of the synthetic receiver functions depicted in Figure 2. On top is a straight stack with no time correction applied. The bottom three receiver function stacks are computed after applying the appropriate normal moveout correction for Ps, P2p1s, and P1p2s respectively (from top to bottom).

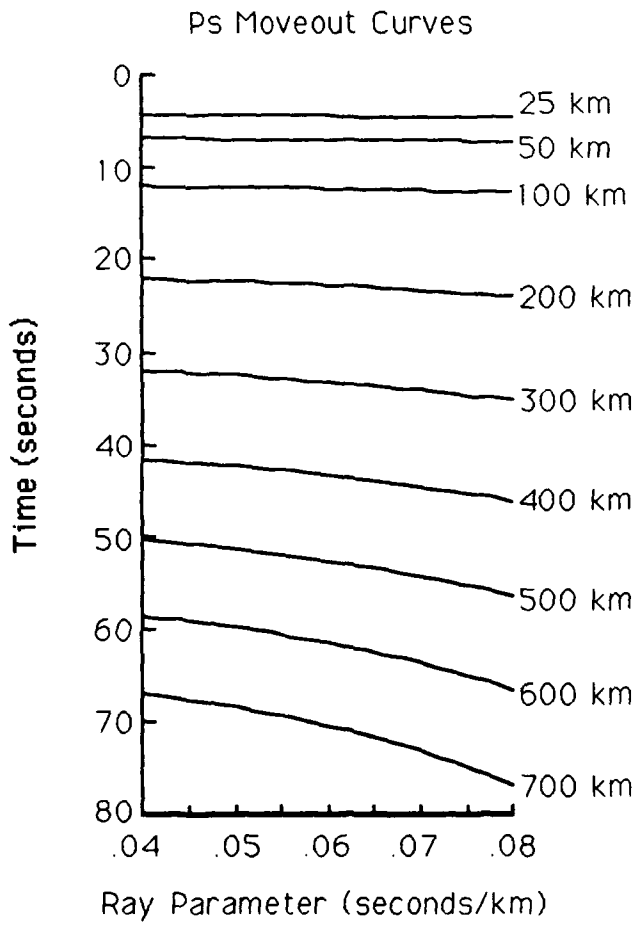

Figure 6. Moveout curves at various depths from 25 km to 700 km for the Ps phase computed for the PREM velocity structure. The depths associated with each curve are printed on the left.

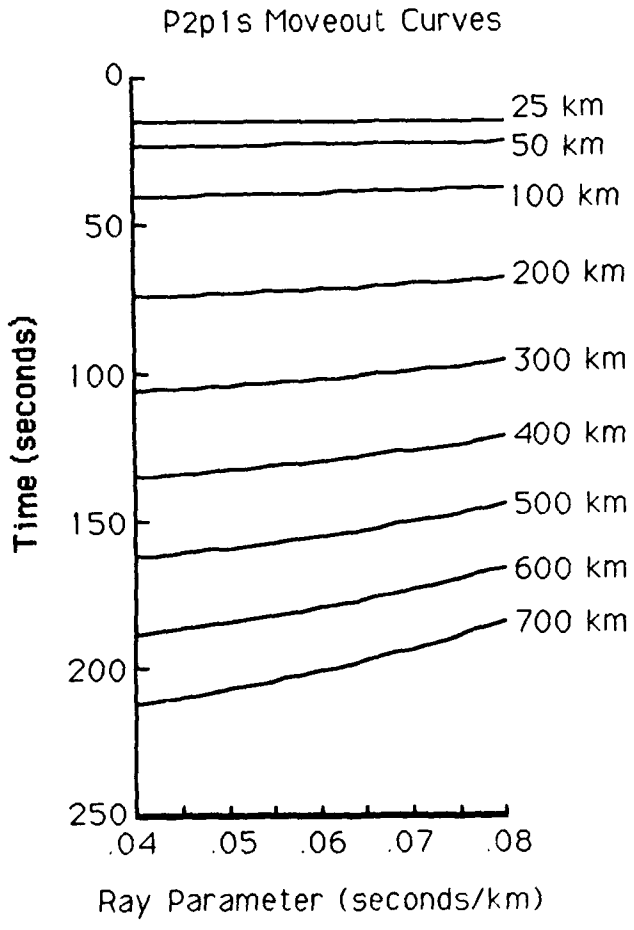

Figure 7. Moveout curves at various depths from 25 km to 700 km for the P2p1s phase computed for the PREM velocity structure. The depths associated with each curve are printed on the left.

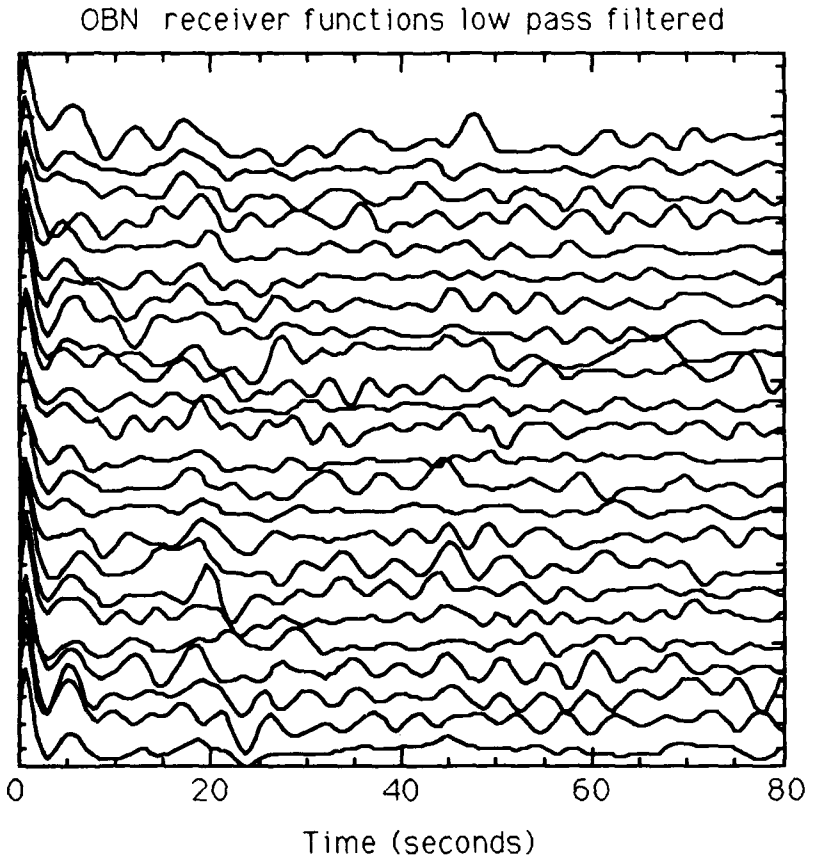

Figure 8. Low pass filtered individual receiver functions computed for OBN. The only clear arrivals without stacking are the Ps conversion from the Moho at 5 seconds and, in a few receiver functions the P2p1s and P1p2s from the Moho at 20 and 23 seconds respectively.

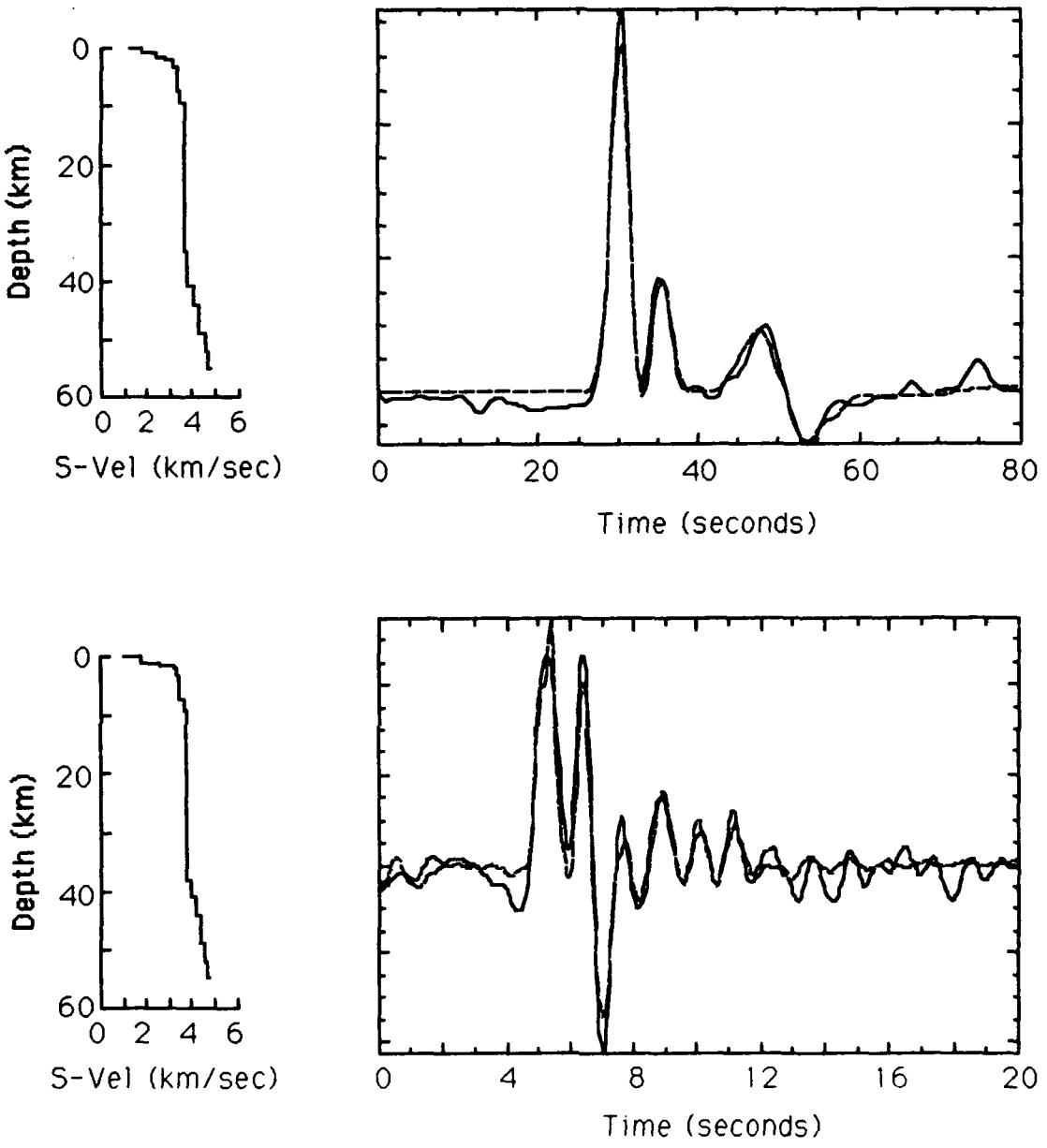

Figure 9. The synthetic (solid line) and observed (dashed line) stacked receiver functions computed for the Soviet Seismographic station at Obninsk. The synthetics pertain to the crustal structure models depicted to the left of the respective receiver functions. The low pass filtered response (stack of the receiver functions given in figure 8) is given on the top figure; the broad band results are on the bottom.

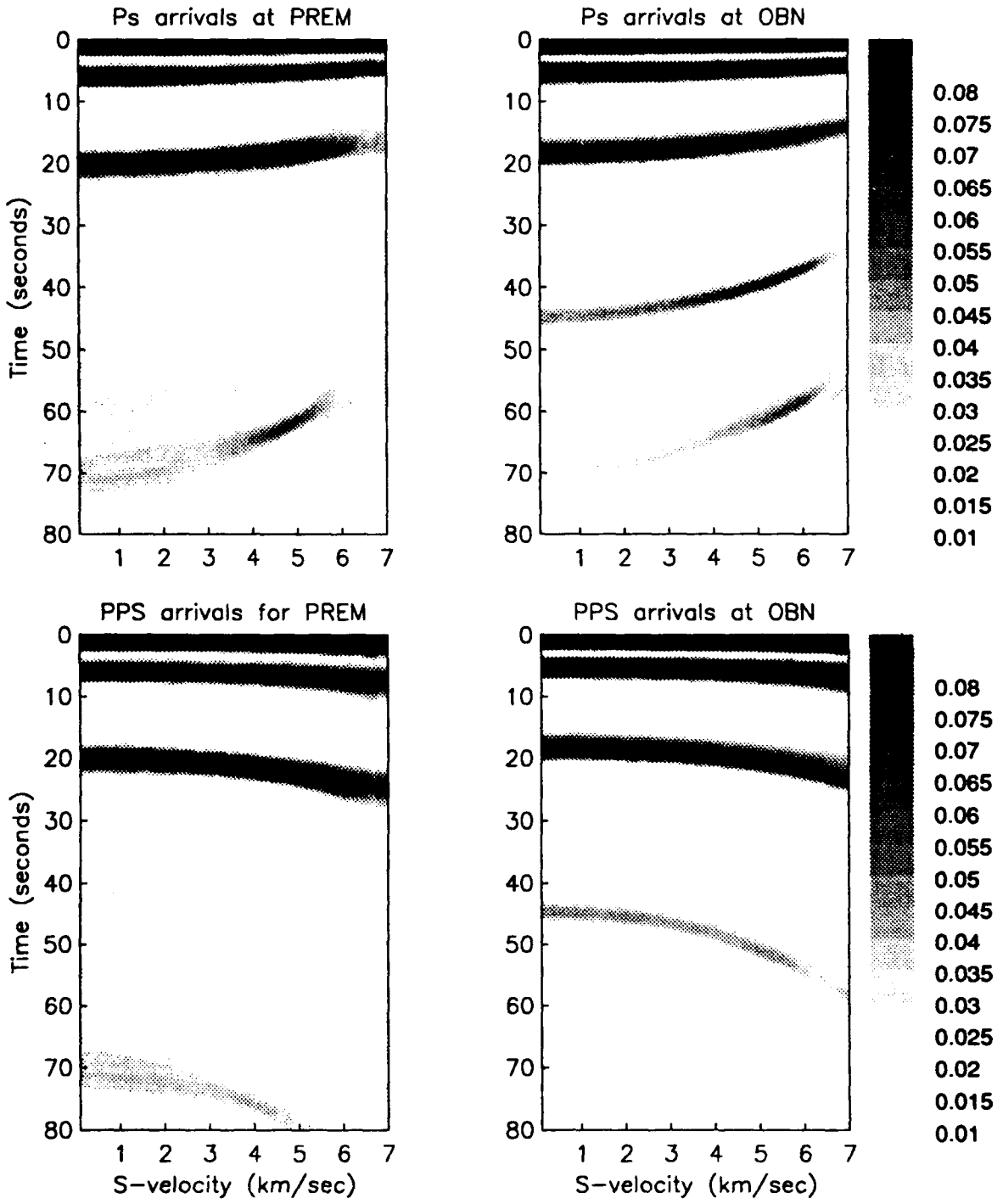

Figure 10. The two top velocity spectrum stacks are produced from the synthetics computed from PREM (left) and receiver functions computed from observed data recorded at Obninsk (right). The two lower plots are the corresponding P2p1s stacks.

Prof. Thomas Ahrens
Seismological Lab, 252-21
Division of Geological & Planetary Sciences
California Institute of Technology
Pasadena, CA 91125

Prof. Keiiti Aki
Center for Earth Sciences
University of Southern California
University Park
Los Angeles, CA 90089-0741

Prof. Shelton Alexander
Geosciences Department
403 Deike Building
The Pennsylvania State University
University Park, PA 16802

Dr. Ralph Alewine, III
DARPA/NMRO
3701 North Fairfax Drive
Arlington, VA 22203-1714

Prof. Charles B. Archambeau
CIRES
University of Colorado
Boulder, CO 80309

Dr. Thomas C. Bache, Jr.
Science Applications Int'l Corp.
10260 Campus Point Drive
San Diego, CA 92121 (2 copies)

Prof. Muawia Barazangi
Institute for the Study of the Continent
Cornell University
Ithaca, NY 14853

Dr. Jeff Barker
Department of Geological Sciences
State University of New York
at Binghamton
Vestal, NY 13901

Dr. Douglas R. Baumgardt
ENSCO, Inc
5400 Port Royal Road
Springfield, VA 22151-2388

Dr. Susan Beck
Department of Geosciences
Building #77
University of Arizona
Tuscon, AZ 85721

Dr. T.J. Bennett
S-CUBED
A Division of Maxwell Laboratories
11800 Sunrise Valley Drive, Suite 1212
Reston, VA 22091

Dr. Robert Blandford
AFTAC/TT, Center for Seismic Studies
1300 North 17th Street
Suite 1450
Arlington, VA 22209-2308

Dr. G.A. Bollinger
Department of Geological Sciences
Virginia Polytechnical Institute
21044 Derring Hall
Blacksburg, VA 24061

Dr. Stephen Bratt
Center for Seismic Studies
1300 North 17th Street
Suite 1450
Arlington, VA 22209-2308

Dr. Lawrence Burdick
Woodward-Clyde Consultants
566 El Dorado Street
Pasadena, CA 91109-3245

Dr. Robert Burridge
Schlumberger-Doll Research Center
Old Quarry Road
Ridgefield, CT 06877

Dr. Jerry Carter
Center for Seismic Studies
1300 North 17th Street
Suite 1450
Arlington, VA 22209-2308

Dr. Eric Chael
Division 9241
Sandia Laboratory
Albuquerque, NM 87185

Prof. Vernon F. Cormier
Department of Geology & Geophysics
U-45, Room 207
University of Connecticut
Storrs, CT 06268

Prof. Steven Day
Department of Geological Sciences
San Diego State University
San Diego, CA 92182

Marvin Denny
U.S. Department of Energy
Office of Arms Control
Washington, DC 20585

Dr. Zoltan Der
ENSCO, Inc.
5400 Port Royal Road
Springfield, VA 22151-2388

Prof. Adam Dziewonski
Hoffman Laboratory, Harvard University
Dept. of Earth Atmos. & Planetary Sciences
20 Oxford Street
Cambridge, MA 02138

Prof. John Ebel
Department of Geology & Geophysics
Boston College
Chestnut Hill, MA 02167

Eric Fielding
SNEE Hall
INSTOC
Cornell University
Ithaca, NY 14853

Dr. Mark D. Fisk
Mission Research Corporation
735 State Street
P.O. Drawer 719
Santa Barbara, CA 93102

Prof Stanley Flatte
Applied Sciences Building
University of California. Santa Cruz
Santa Cruz, CA 95064

Dr. John Foley
NER-Geo Sciences
1100 Crown Colony Drive
Quincy, MA 02169

Prof. Donald Forsyth
Department of Geological Sciences
Brown University
Providence, RI 02912

Dr. Art Frankel
U.S. Geological Survey
922 National Center
Reston, VA 22092

Dr. Cliff Frolich
Institute of Geophysics
8701 North Mopac
Austin, TX 78759

Dr. Holly Given
IGPP, A-025
Scripps Institute of Oceanography
University of California, San Diego
La Jolla, CA 92093

Dr. Jeffrey W. Given
SAIC
10260 Campus Point Drive
San Diego, CA 92121

Dr. Dale Glover
Defense Intelligence Agency
ATTN: ODT-1B
Washington, DC 20301

Dr. Indra Gupta
Teledyne Geotech
314 Montgomery Street
Alexanderia, VA 22314

Dan N. Hagedon
Pacific Northwest Laboratories
Battelle Boulevard
Richland, WA 99352

Dr. James Hannon
Lawrence Livermore National Laboratory
P.O. Box 808
L-205
Livermore, CA 94550

Dr. Roger Hansen
HQ AFTAC/TTR
Patrick AFB, FL 32925-6001

Prof. David G. Harkrider
Seismological Laboratory
Division of Geological & Planetary Sciences
California Institute of Technology
Pasadena, CA 91125

Prof. Danny Harvey
CIRES
University of Colorado
Boulder, CO 80309

Prof. Donald V. Helmberger
Seismological Laboratory
Division of Geological & Planetary Sciences
California Institute of Technology
Pasadena, CA 91125

Prof. Eugene Herrin
Institute for the Study of Earth and Man
Geophysical Laboratory
Southern Methodist University
Dallas, TX 75275

Prof. Robert B. Herrmann
Department of Earth & Atmospheric Sciences
St. Louis University
St. Louis, MO 63156

Prof. Lane R. Johnson
Seismographic Station
University of California
Berkeley, CA 94720

Prof. Thomas H. Jordan
Department of Earth, Atmospheric &
Planetary Sciences
Massachusetts Institute of Technology
Cambridge, MA 02139

Prof. Alan Kafka
Department of Geology & Geophysics
Boston College
Chestnut Hill, MA 02167

Robert C. Kemerait
ENSCO, Inc.
445 Pineda Court
Melbourne, FL 32940

Dr. Max Koontz
U.S. Dept. of Energy/DP 5
Forrestal Building
1000 Independence Avenue
Washington, DC 20585

Dr. Richard LaCoss
MIT Lincoln Laboratory, M-200B
P.O. Box 73
Lexington, MA 02173-0073

Dr. Fred K. Lamb
University of Illinois at Urbana-Champaign
Department of Physics
1110 West Green Street
Urbana, IL 61801

Prof. Charles A. Langston
Geosciences Department
403 Deike Building
The Pennsylvania State University
University Park, PA 16802

Jim Lawson, Chief Geophysicist
Oklahoma Geological Survey
Oklahoma Geophysical Observatory
P.O. Box 8
Leonard, OK 74043-0008

Prof. Thorne Lay
Institute of Tectonics
Earth Science Board
University of California, Santa Cruz
Santa Cruz, CA 95064

Dr. William Leith
U.S. Geological Survey
Mail Stop 928
Reston, VA 22092

Mr. James F. Lewkowicz
Phillips Laboratory/GPEH
Hanscom AFB, MA 01731-5000(2 copies)

Mr. Alfred Lieberman
ACDA/VI-OA State Department Building
Room 5726
320-21st Street, NW
Washington, DC 20451

Prof. L. Timothy Long
School of Geophysical Sciences
Georgia Institute of Technology
Atlanta, GA 30332

Dr. Randolph Martin, III
New England Research, Inc.
76 Olcott Drive
White River Junction, VT 05001

Dr. Robert Masse
Denver Federal Building
Box 25046, Mail Stop 967
Denver, CO 80225

Dr. Gary McCartor
Department of Physics
Southern Methodist University
Dallas, TX 75275

Prof. Thomas V. McEvilly
Seismographic Station
University of California
Berkeley, CA 94720

Dr. Art McGarr
U.S. Geological Survey
Mail Stop 977
U.S. Geological Survey
Menlo Park, CA 94025

Dr. Keith L. McLaughlin
S-CUBED
A Division of Maxwell Laboratory
P.O. Box 1620
La Jolla, CA 92038-1620

Stephen Miller & Dr. Alexander Florence
SRI International
333 Ravenswood Avenue
Box AF 116
Menlo Park, CA 94025-3493

Prof. Bernard Minster
IGPP, A-025
Scripps Institute of Oceanography
University of California, San Diego
La Jolla, CA 92093

Prof. Brian J. Mitchell
Department of Earth & Atmospheric Sciences
St. Louis University
St. Louis, MO 63156

Mr. Jack Murphy
S-CUBED
A Division of Maxwell Laboratory
11800 Sunrise Valley Drive, Suite 1212
Reston, VA 22091 (2 Copies)

Dr. Keith K. Nakanishi
Lawrence Livermore National Laboratory
L-025
P.O. Box 808
Livermore, CA 94550

Dr. Carl Newton
Los Alamos National Laboratory
P.O. Box 1663
Mail Stop C335, Group ESS-3
Los Alamos, NM 87545

Dr. Bao Nguyen
HQ AFTAC/TTR
Patrick AFB, FL 32925-6001

Prof. John A. Orcutt
IGPP, A-025
Scripps Institute of Oceanography
University of California, San Diego
La Jolla, CA 92093

Prof. Jeffrey Park
Kline Geology Laboratory
P.O. Box 6666
New Haven, CT 06511-8130

Dr. Howard Patton
Lawrence Livermore National Laboratory
L-025
P.O. Box 808
Livermore, CA 94550

Dr. Frank Pilotte
HQ AFTAC/TT
Patrick AFB, FL 32925-6001

Dr. Jay J. Pulli
Radix Systems, Inc.
2 Taft Court, Suite 203
Rockville, MD 20850

Dr. Robert Reinke
ATTN: FCTVTD
Field Command
Defense Nuclear Agency
Kirtland AFB, NM 87115

Prof. Paul G. Richards
Lamont-Doherty Geological Observatory
of Columbia University
Palisades, NY 10964

Mr. Wilmer Rivers
Teledyne Geotech
314 Montgomery Street
Alexandria, VA 22314

Dr. George Rothe
HQ AFTAC/TTR
Patrick AFB, FL 32925-6001

Dr. Alan S. Ryall, Jr.
DARPA/NMRO
3701 North Fairfax Drive
Arlington, VA 22209-1714

Dr. Richard Sailor
TASC, Inc.
55 Walkers Brook Drive
Reading, MA 01867

Prof. Charles G. Sammis
Center for Earth Sciences
University of Southern California
University Park
Los Angeles, CA 90089-0741

Prof. Christopher H. Scholz
Lamont-Doherty Geological Observatory
of Columbia University
Palisades, CA 10964

Dr. Susan Schwartz
Institute of Tectonics
1156 High Street
Santa Cruz, CA 95064

Secretary of the Air Force
(SAFRD)
Washington, DC 20330

Office of the Secretary of Defense
DDR&E
Washington, DC 20330

Thomas J. Sereno, Jr.
Science Application Int'l Corp.
10260 Campus Point Drive
San Diego, CA 92121

Dr. Michael Shore
Defense Nuclear Agency/SPSS
6801 Telegraph Road
Alexandria, VA 22310

Dr. Matthew Sibol
Virginia Tech
Seismological Observatory
4044 Derring Hall
Blacksburg, VA 24061-0420

Prof. David G. Simpson
IRIS, Inc.
1616 North Fort Myer Drive
Suite 1440
Arlington, VA 22209

Donald L. Springer
Lawrence Livermore National Laboratory
L-025
P.O. Box 808
Livermore, CA 94550

Dr. Jeffrey Stevens
S-CUBED
A Division of Maxwell Laboratory
P.O. Box 1620
La Jolla, CA 92038-1620

Lt. Col. Jim Stobie
ATTN: AFOSR/NL
Bolling AFB
Washington, DC 20332-6448

Prof. Brian Stump
Institute for the Study of Earth & Man
Geophysical Laboratory
Southern Methodist University
Dallas, TX 75275

Prof. Jeremiah Sullivan
University of Illinois at Urbana-Champaign
Department of Physics
1110 West Green Street
Urbana, IL 61801

Prof. L. Sykes
Lamont-Doherty Geological Observatory
of Columbia University
Palisades, NY 10964

Dr. David Taylor
ENSCO, Inc.
445 Pineda Court
Melbourne, FL 32940

Dr. Steven R. Taylor
Los Alamos National Laboratory
P.O. Box 1663
Mail Stop C335
Los Alamos, NM 87545

Prof. Clifford Thurber
University of Wisconsin-Madison
Department of Geology & Geophysics
1215 West Dayton Street
Madison, WS 53706

Prof. M. Nafi Toksoz
Earth Resources Lab
Massachusetts Institute of Technology
42 Carleton Street
Cambridge, MA 02142

Dr. Larry Turnbull
CIA-OSWR/NED
Washington, DC 20505

Dr. Gregory van der Vink
IRIS, Inc.
1616 North Fort Myer Drive
Suite 1440
Arlington, VA 22209

Dr. Karl Veith
EG&G
5211 Auth Road
Suite 240
Suitland, MD 20746

Prof. Terry C. Wallace
Department of Geosciences
Building #77
University of Arizona
Tuscon, AZ 85721

Dr. Thomas Weaver
Los Alamos National Laboratory
P.O. Box 1663
Mail Stop C335
Los Alamos, NM 87545

Dr. William Wortman
Mission Research Corporation
8560 Cinderbed Road
Suite 700
Newington, VA 22122

Prof. Francis T. Wu
Department of Geological Sciences
State University of New York
at Binghamton
Vestal, NY 13901

AFTAC/CA
(STINFO)
Patrick AFB, FL 32925-6001

DARPA/PM
3701 North Fairfax Drive
Arlington, VA 22203-1714

DARPA/RMO/RETRIEVAL
3701 North Fairfax Drive
Arlington, VA 22203-1714

DARPA/RMO/SECURITY OFFICE
3701 North Fairfax Drive
Arlington, VA 22203-1714

HQ DNA
ATTN: Technical Library
Washington, DC 20305

Defense Intelligence Agency
Directorate for Scientific & Technical Intelligence
ATTN: DTIB
Washington, DC 20340-6158

Defense Technical Information Center
Cameron Station
Alexandria, VA 22314 (2 Copies)

TACTEC
Battelle Memorial Institute
505 King Avenue
Columbus, OH 43201 (Final Report)

Phillips Laboratory
ATTN: XPG
Hanscom AFB, MA 01731-5000

Phillips Laboratory
ATTN: GPE
Hanscom AFB, MA 01731-5000

Phillips Laboratory
ATTN: TSML
Hanscom AFB, MA 01731-5000

Phillips Laboratory
ATTN: SUL
Kirtland, NM 87117 (2 copies)

Dr. Michel Bouchon
I.R.I.G.M.-B.P. 68
38402 St. Martin D'Heres
Cedex, FRANCE

Dr. Michel Campillo
Observatoire de Grenoble
I.R.I.G.M.-B.P. 53
38041 Grenoble, FRANCE

Dr. Kin Yip Chun
Geophysics Division
Physics Department
University of Toronto
Ontario, CANADA

Prof. Hans-Peter Harjes
Institute for Geophysic
Ruhr University/Bochum
P.O. Box 102148
4630 Bochum 1, GERMANY

Prof. Eystein Husebye
NTNF/NORSAR
P.O. Box 51
N-2007 Kjeller, NORWAY

David Jepsen
Acting Head, Nuclear Monitoring Section
Bureau of Mineral Resources
Geology and Geophysics
G.P.O. Box 378, Canberra, AUSTRALIA

Ms. Eva Johannisson
Senior Research Officer
National Defense Research Inst.
P.O. Box 27322
S-102 54 Stockholm, SWEDEN

Dr. Peter Marshall
Procurement Executive
Ministry of Defense
Blacknest, Brimpton
Reading FG7-FRS, UNITED KINGDOM

Dr. Bernard Massinon, Dr. Pierre Mechler
Societe Radiomana
27 rue Claude Bernard
75005 Paris, FRANCE (2 Copies)

Dr. Svein Mykkeltveit
NTNT/NORSAR
P.O. Box 51
N-2007 Kjeller, NORWAY (3 Copies)

Prof. Keith Priestley
University of Cambridge
Bullard Labs, Dept. of Earth Sciences
Madingley Rise, Madingley Road
Cambridge CB3 OEZ, ENGLAND

Dr. Jorg Schlittenhardt
Federal Institute for Geosciences & Nat'l Res.
Postfach 510153
D-3000 Hannover 51, GERMANY

Dr. Johannes Schweitzer
Institute of Geophysics
Ruhr University/Bochum
P.O. Box 1102148
4360 Bochum 1, GERMANY